Relationship between cumulus activity and environmental moisture during the CINDY2011/DYNAMO field experiment as revealed from convection-resolving simulations

AUTHOR(S):

Takemi, Tetsuya

CITATION:

Takemi, Tetsuya. Relationship between cumulus activity and environmental moisture during the CINDY2011/DYNAMO field experiment as revealed from convection-resolving simulations. Journal of the Meteorological Society of Japan 2016, 93A: 41-58

ISSUE DATE:

2016-01-20

URL:

http://hdl.handle.net/2433/211194

Journal of the Meteorological Society of Japan, Vol. 93A, pp. 41−58, 2015
DOI:10.2151/jmsj.2015-035

Relationship between Cumulus Activity and Environmental Moisture during the CINDY2011/DYNAMO Field Experiment as Revealed from Convection-Resolving Simulations

Tetsuya TAKEMI

Disaster Prevention Research Institute, Kyoto University, Uji, Japan

(Manuscript received 9 February 2015, in final form 22 May 2015)

Abstract

The cumulus convection activity in the tropical oceanic regions is strongly regulated by the large-scale environmental atmosphere, while at the same time, cumulus convection will influence the large-scale atmosphere. It is thus recognized that the spatiotemporal variability of moisture content plays an important role in determining such multiscale interaction processes relevant to tropical cumulus convection. This study investigates the relationship between cumulus convection and environmental moisture in the tropical Indian Ocean by conducting convection-resolving simulations through the nesting capability with which the innermost domain has the 100 m grid resolution. We examine the cases observed from October to November 2011 during the Cooperative Indian Ocean Experiment on Intraseasonal Variability in the Year 2011/Dynamics of the Madden–Julian oscillation (MJO) field experiment. Based on the favorable performance of the outermost domain simulations in reproducing eastward propagating signals over the Indian Ocean, the data obtained from the 100 m mesh simulations are examined. It is shown that the cloud cover whose tops exceed a middle level sharply increases with the increase in precipitable water vapor over about 55 mm. The increase in relative humidity in a lower layer results in the increase in cloud cover at a level above the humid layer. From the convection-resolving simulations, the existence of updraft cores that are less diluted with the environment is demonstrated. It is considered that cloud-core parcels are less susceptible to the negative effects of dilution with the environment and survive to penetrate to upper levels, which contributes to the moistening of the environmental atmosphere. The existence of updraft cores plays a key role in the inter-relationship between cumulus convection and its environment. The effects from cumulus clouds on their environment are regarded as a preconditioning influence for the convective initiation of MJO.

Keywords tropical meteorology; cumulus convection; convection-resolving simulations; moisture variability; cumulus preconditioning; CINDY2011/DYNAMO

1. Introduction

Cumulus clouds in the tropical oceanic regions develop in response to the spatiotemporal variability of atmospheric stability, wind shear, and sea surface temperature. With favorable conditions, cumulus clouds organize into mesoscale convective systems, cloud clusters, and in some cases tropical cyclones. Furthermore, the organization of cumulus clouds is considered to play a key role in forming intra-seasonal oscillation coupled with deep convective activity, which is known as the Madden–Julian oscillation (MJO) (Madden and Julian 1971, 1972). Even though numerous studies have been conducted on MJO, there still remain unsolved issues on the mechanisms for MJO development and on the skills in predicting MJO with global weather forecasting models (Zhang 2005).

Corresponding author: Tetsuya Takemi, Disaster Prevention Research Institute, Kyoto University, Gokasho, Uji, Kyoto 611-0011, Japan
E-mail: takemi@storm.dpri.kyoto-u.ac.jp

Cumulus clouds themselves have various development modes, i.e., shallow cumulus, cumulus congestus, and cumulonimbus (Johnson et al. 1999), which are characterized by the vertical development of convection. These cumulus modes are controlled by stratification as well as moisture. In particular, a stably stratified layer at middle levels, which is formed by the detrainment processes of deep convection, will control the vertical development of cumulus clouds (Zuidema 1998). In addition, the cumulus modes are regulated by the moisture variability of the tropical atmosphere. The tropical atmosphere generally has only a minor temperature gradient in the horizontal direction because of the absence of baroclinicity, while it frequently has a large change in moisture content not only in the vertical but also in the horizontal direction. A large moisture variability can be seen over the tropical western Pacific (Yoneyama 2003) and the tropical Indian Ocean (Yoneyama et al. 2008). Such a large moisture variability is considered to influence the development of cumulus modes (Brown and Zhang 1997; Takemi et al. 2004; Derbyshire et al. 2004; Jensen and Del Genio 2006; Kumar et al. 2014). Thus, cumulus convection activity in the tropical oceanic regions is strongly regulated by stratification and moisture that are characterized by large-scale atmospheric variability including MJO.

On the other hand, cumulus clouds transport moisture upward and therefore should have feedback effects on the surrounding atmosphere through moistening. This feedback is considered to play a role in the development of following deep convection by preconditioning the atmosphere favorable for the deep convection. Recent studies have tackled this preconditioning issue to gain insights in the initiation processes of MJO (Waite and Khouider 2010; Rapp et al. 2011; Del Genio et al. 2012; Hohenegger and Stevens 2013; Hagos et al. 2014; Ruppert and Johnson 2015).

The roles of moisture variability in activating processes that would lead to MJO initiation have been one of the major research issues in recent studies. To enhance and advance our understanding of the processes relevant to MJO initiation, a field experiment over the Indian Ocean in 2011–2012 was organized under the Cooperative Indian Ocean Experiment on Intraseasonal Variabiilty in the Year 2011 (CINDY2011) and Dynamics of the MJO (DYNAMO) (Zhang et al. 2013; Yoneyama et al. 2013). One of the key objectives in CINDY2011/DYNAMO is to reveal MJO initiation and propagation through convective processes including congestus preconditioning for the transition to deep convection.

Recent studies investigated cumulus convection and moisture variability in the tropical regions and for MJO initiation with numerical simulations at *O* (1 km) resolutions (Hagos et al. 2013, 2014; Holloway et al. 2013), known as cloud-permitting simulations. However, to investigate convective initiation processes, we need to conduct higher resolution simulations that sufficiently resolve cumulus convection and explicitly represent interacting processes between cumulus clouds and their environments. In this study, we focus on the relationship between cumulus clouds and environmental moisture during the field experiment of CINDY2011/DYNAMO by employing an approach of convection-resolving simulation at the 100 m grid spacing.

In general, tropical cumulus clouds have weaker updrafts with smaller buoyancy than the mid-latitude counterparts (Zipser and LeMone 1980; Jorgensen and LeMone 1989; Lucas et al. 1994a, b; Igau et al. 1999). During slower ascent under smaller buoyancy in the tropical oceanic environments, air parcels in cumulus clouds will be diluted and mixed with environmental air, which leads to suppress the vertical growth of cumulus clouds. Takemi (2014) demonstrated the sensitivity of the intensity of convective systems to temperature lapse rate by comparing those simulated in the tropical, oceanic, and the mid-latitude continental environment. In addition, the vertical development of tropical cumulus clouds is sensitively regulated by environmental humidity profiles (Takemi et al. 2004): a moister condition in a deeper tropospheric layer is beneficial for deeper clouds. It is considered that cumulus clouds that gradually develop in the vertical will provide moisture in upper levels by mixing with the environment, i.e., preconditioning effects. In other words, cumulus convection activity in the tropical oceanic regions is strongly regulated by the large-scale environmental atmosphere, while at the same time, cumulus convection influences the large-scale atmosphere. It is recognized that the spatiotemporal variability of moisture content plays an important role in determining such multi-scale interaction processes: the down-scale control on cumulus convection and up-scale influence on the environmental atmosphere.

In this study, we investigate the relationship between cumulus activity and environmental moisture in the tropical Indian Ocean during October and November 2011 by conducting 100 m mesh numerical simulations with a non-hydrostatic atmospheric

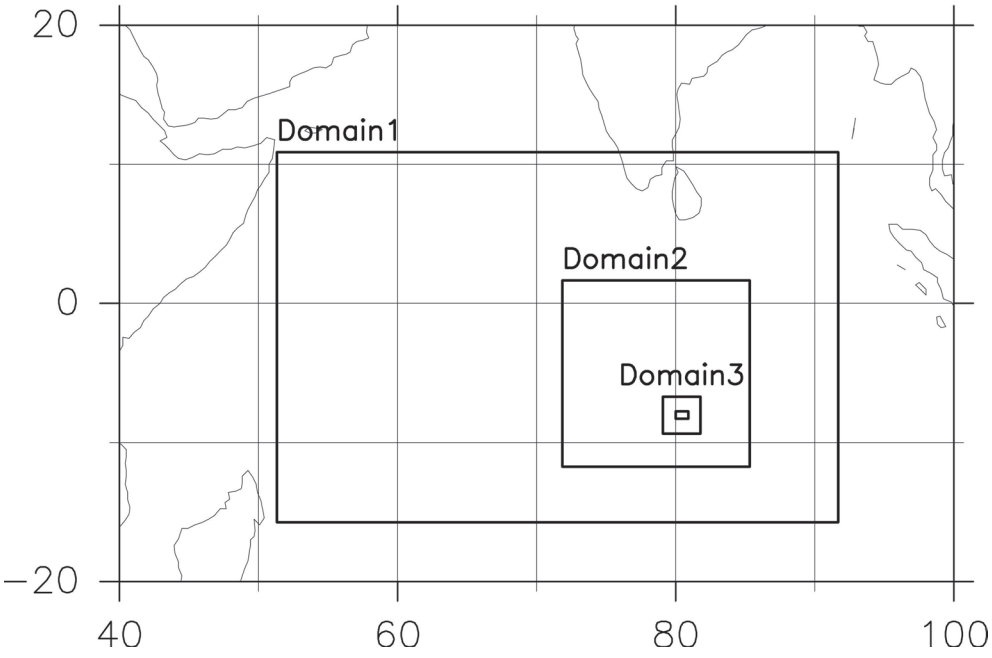

Fig. 1. Four computational domains with the use of the nesting capability of the WRF model. Domain 1 is the outermost domain, within which the three nested domains are set. The innermost domain, i.e., Domain 4, indicated by the smallest rectangular box, is located within Domain 3.

model. The use of this high resolution is intended to sufficiently resolve cumulus clouds (Bryan et al. 2003; Takemi and Rotunno, 2003; Takemi 2008, 2012), and the resolution can be regarded as a convection-resolving range. By employing the nesting capability of the atmospheric model, the computational domains cover the entire tropical Indian Ocean down to a mesoscale region surrounding the stationary observation point of the R/V Mirai of Japan Agency for Marine-Earth Science and Technology (JAMSTEC) during the observation cruise from 1 October to 1 December in 2011 as a part of the CINDY2011/DYNAMO field campaign. During this time period, two MJOs occurred over the Indian Ocean: one in late October to early November and the other in late November to early December, which were well documented observationally by Johnson and Ciesielski (2013) and Gottschalck et al. (2013) and numerically by Nasuno (2013) and Fu et al. (2013) with global models. The present analyses are made on the mesoscale region around the R/V Mirai observation point to examine the effects of sufficiently resolved cumulus convection on the environmental atmosphere. In this study, large-scale atmospheric variations are regarded as a prescribed background condition for cumulus activity in the mesoscale region. We will investigate the role of cumulus convection in moistening the environmental atmosphere.

2. Numerical model and simulation setup

The numerical model used here is a version of the Weather Research and Forecasting (WRF) model, the Advanced Research WRF (ARW) version 3.3.1 (Skamarock et al. 2008). The WRF model is a non-hydrostatic, compressible atmospheric model that is used in various meteorological applications. In this study, we conduct numerical simulations of the tropospheric variability and cumulus convection as observed over the tropical Indian Ocean during October and November in 2011 as a part of the CINDY2011/DYNAMO field experiment. For this purpose, we configure the WRF model in a realistic mode.

We employ the nesting capability of the WRF model to conduct convection-resolving simulations that sufficiently resolve cumulus clouds in the finest resolution domain. Since the focus in the present analysis is placed on the region surrounding the stationary observation site of the R/V Mirai, the nested domains are set, as shown in Fig. 1. The outermost domain, i.e., Domain 1, has an area of 4250 km × 3000 km

(longitude range: 51.3°E to 91.7°E; latitude range: 15.7°S to 10.9°N) at the 12.5 km grid spacing, which covers most of the tropical Indian Ocean. The area size and the horizontal grid spacing of the inner two domains, i.e., Domains 2 and 3, are 1500 km × 1500 km (71.85°E to 85.32°E, 11.74°S to 1.65°N) at the 2.5 km grid and 300 km × 300 km (79.08°E to 81.77°E, 9.36°S to 6.69°N) at the 500 m grid, respectively. The innermost domain, i.e., Domain 4, is nested within Domain 3 and has an area of 100 km × 60 km (80.009°E to 80.908°E, 8.282°S to 7.748°S) at the 100 m grid. Domains 3 and 4 are centered at the R/V Mirai observation site (80.5°E, 8°S). The computational areas are configured with the Mercator map projection. There are 62 vertical levels, with the interval being stretched in the vertical. The top of the computational domains is set to be 50 hPa.

Since the present simulations are performed in a realistic mode, all the physics processes are included. We choose physics parameterization schemes by considering the schemes' elaboration and the computational efficiency because we conduct the 100 m resolution simulations for two months. Cloud and precipitation processes are parameterized as follows: a single-moment, six category microphysics scheme of Hong and Lim (2006) and a revised Tiedtke's (1989) cumulus parameterization scheme of Zhang et al. (2011) (but applied only for Domain 1). For boundary layer mixing, a non-local mixing scheme of Hong et al. (2006) is employed for Domains 1, 2, and 3. On the other hand, a subgrid-scale model of Deardorff (1980) is used for representing turbulent mixing in Domain 4 simulations. For radiation parameterizations, a simple downward scheme of Dudhia (1989) for shortwave radiation and the rapid radiative transfer model of Mlawer et al. (1997) for longwave radiation are used.

To prescribe the initial and boundary conditions of the WRF model, we use six-hourly operational global analysis (GANAL) data of Japan Meteorological Agency (JMA) for the atmosphere and Merged satellite and in situ data global daily sea surface temperature (MGDSST) data of JMA for sea surface temperature. The GANAL data have a spatial resolution of 0.5° and 23 levels in the vertical, whereas the MGDSST data have a resolution of 0.25°. The daily MGDSST data are linearly interpolated at an interval of 6 h to be the same with the time interval of GANAL. Terrain and land–ocean contrast in the computation domain are determined with the use of GTOPO30 and Global Land Cover Characterization datasets.

The numerical simulations for the analyses are conducted from 0000 UTC 1 October 2011 to 0000 UTC, corresponding to the intensive observation period of the R/V Mirai. To prevent the large-scale atmospheric variability away from the GANAL fields, we conduct numerical simulations by segmenting the two-month period into two-day interval with one day shifted. The initial time of each two-day segment is 0000 UTC on day X. Each segmented simulation is initiated from the computation of Domain 1, followed by the computations of the nested domains, i.e., the initial times of Domains 2, 3, and 4 are 1200 UTC on day X, 1800 UTC on day X, and 0000 UTC on day X + 1, respectively. All the computations from the outermost to the innermost domain in each segmented simulation are terminated at 0000 UTC on day X + 2. The outputs from 0000 UTC on day X + 1 to 0000 UTC on day X + 2 are used for the present analyses. For example, the simulated data are obtained from the segmented simulation initiated at 0000 UTC 30 September 2011 in Domain 1, at 1200 UTC 30 September in Domain 2, at 1800 UTC 30 September in Domain 3, and at 0000 UTC 1 October in Domain 4 until 0000 UTC 1 October 2011. Overall, 61 segmented simulations are conducted starting from 0000 UTC 30 September 2011, and ending at 0000 UTC 1 December 2011, and the outputs from 0000 UTC 1 October to 0000 UTC 1 December are used. All the computational domains are connected in one way, which means that the meteorological variables are passed on from a mother domain to a child domain. The time intervals of the data outputs are 60 min for Domains 1 and 2 and 5 min for Domains 3 and 4.

3. Results

3.1 Overall characteristics of the simulated atmosphere: Comparison with the observations

First, the overall characteristics of the simulated fields are presented through the comparison with the observations. The comparison here is made in terms of moisture variables because moisture highly fluctuates in time and space depending on large-scale atmospheric variability and cumulus activity.

Figure 2 shows the time and height diagram of relative humidity obtained from three-hourly radiosonde observations at the R/V Mirai site from 0000 UTC 1 October to 0000 UTC 1 December in 2011. The details of the radiosonde observations can be found in the studies of Yoneyama et al. (2013) and Ciesielski et al. (2014). Higher humidity exceeding 80 % at the lowest 2 km layer can continuously be

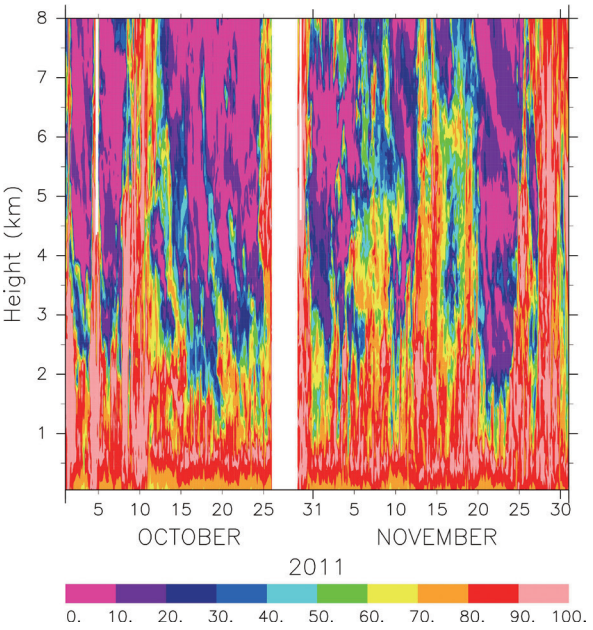

Fig. 2. Time and height diagram of relative humidity (%) obtained from the radiosonde observations at the R/V Mirai site from 0000 UTC 1 October to 0000 UTC 1 December in 2011.

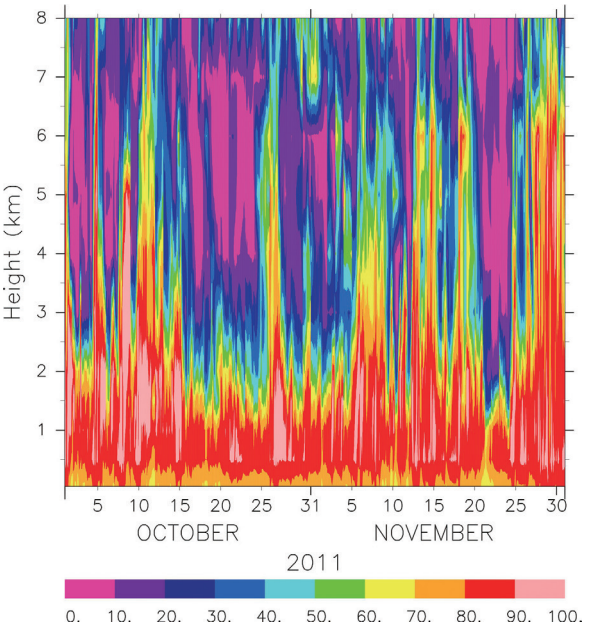

Fig. 3. The same as Fig. 2, except for the results obtained from the simulations in Domain 4. The relative humidity is horizontally averaged over the Domain 4 area.

seen throughout the period, with some sporadic drier conditions. In contrast, higher humidity conditions at the upper levels above the 3 km height occur less frequently. In particular, higher humidity above the 5 km height can be seen on 7–10 October, on a couple of days toward the end of October, in mid-November, and on several days until the end of November. The moister conditions on days in late October and late November correspond to the two MJO events (Johnson and Ciesielski 2013; Gottschalck et al. 2013).

The representation of these observed characteristics of relative humidity is examined from the simulated outputs in Domain 4. Figure 3 shows the time and height diagram of relative humidity horizontally averaged over Domain 4. It is seen that there are persistent higher moisture conditions (but with some sporadic breaks) below the 2 km height, less frequent moist conditions above the 3 km height, and the four moister events above the 5 km height, which agree well with the observed features, as shown in Fig. 2. It was also found that there were good performances of the simulations with the observations in terms of other meteorological variables.

The moisture condition is further examined in terms of precipitable water vapor. Figure 4 compares the time series of precipitable water vapor between the observations and simulations. Corresponding to the moister conditions at the upper levels, as seen in Figs. 2 and 3, higher precipitable water is seen in the early to mid-October, the later period of October, the mid-November, and the later period of November. The simulations adequately capture these moister conditions as well as the temporal variations including drier conditions as observed during the period.

From the comparisons indicated by Figs. 2, 3, and 4, it is shown that the simulations successfully reproduce the observed variability at least in the Domain 4 area. In the following, the large-scale atmospheric variations in the tropical Indian Ocean are examined. During October and November 2011, two MJO events occurred (Johnson and Ciesielski 2013; Gottschalck et al. 2013). Thus, the simulated results obtained in Domain 1 are examined whether eastward propagation of disturbances is seen.

Large-scale atmospheric variability represented in the simulations is examined in terms of the longitude and time diagrams of precipitable water vapor and vertical velocity at the 4 km height, as shown in Fig. 5. The values in this diagram are averaged

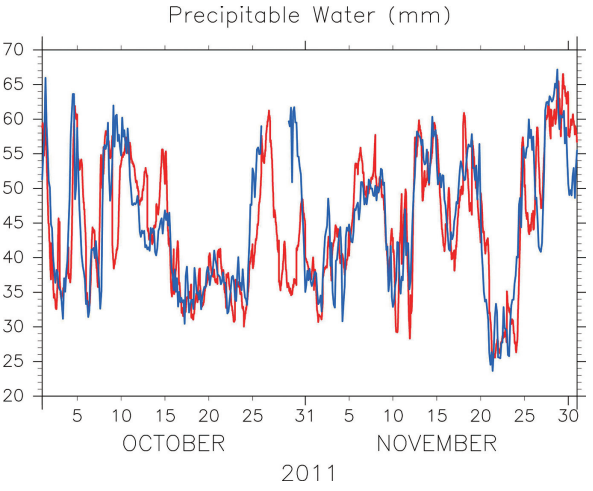

Fig. 4. Time series of precipitable water vapor (in mm) obtained from the Mirai observations (indicated by blue line) and the simulations in Domain 4 (red line). The simulated values are calculated by taking the horizontal averages over the computational area.

in the north and south direction between 5°N and 5°S. Moister signals propagate eastward starting at 50–60°E in mid-October and mid-November passing through the 80.5°E longitude and exiting at the east end of Domain 1. These two eastward propagating signals correspond to two MJO events observed during the time period. Extremely moist conditions are embedded within the MJO events to the east of around the 75°E longitude (Fig. 5a). Associated with these eastward propagating moist signals, upward motion dominates in the tropical Indian Ocean. Considering that the values indicated in Fig. 5 are averaged in the 10° latitude band, the upward motion exceeding 7 cm s^{-1} seen within the MJO signals (Fig. 5b) is regarded as strong large-scale ascent. In Fig. 5b, a sharp signal of such intense ascent that propagates eastward is seen in regions to the east of 75°E longitude in later November, corresponding to the very moist conditions seen in Fig. 5a.

From the results shown in Fig. 5, it is indicated that the simulations successfully reproduce the eastward propagating signals that are induced by MJO. By confirming the favorable performance of the vertical structure at the Mirai site as well as the large-scale fields we will investigate cumulus activity under prescribed large-scale conditions that are realistically represented.

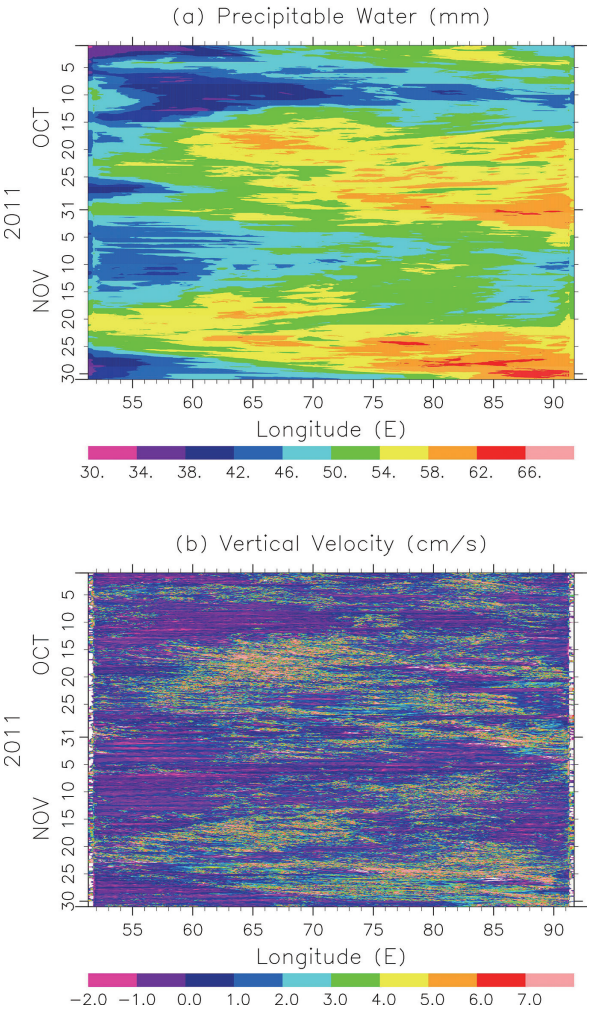

Fig. 5. Longitude and time diagrams of (a) precipitable water vapor (in mm) and (b) vertical velocity (in cm s^{-1}) at the height of 4 km averaged in latitude between 5°N and 5°S from 0000 UTC 1 October to 0000 UTC 1 December 2011. The times indicated on the vertical axis progress downward.

3.2 *Cumulus activity and environmental stability conditions*

In this section, we investigate the relationship between cumulus clouds and environmental conditions by using the outputs at 5 min interval produced in the Domain 4 simulations. In general, the development of cumulus convection is strongly regulated by environmental stability. Since the development of cumulus convection may depend on temperature lapse rate and relative humidity (Takemi et al. 2004; Takemi 2007a, b, 2010), these parameters are examined first.

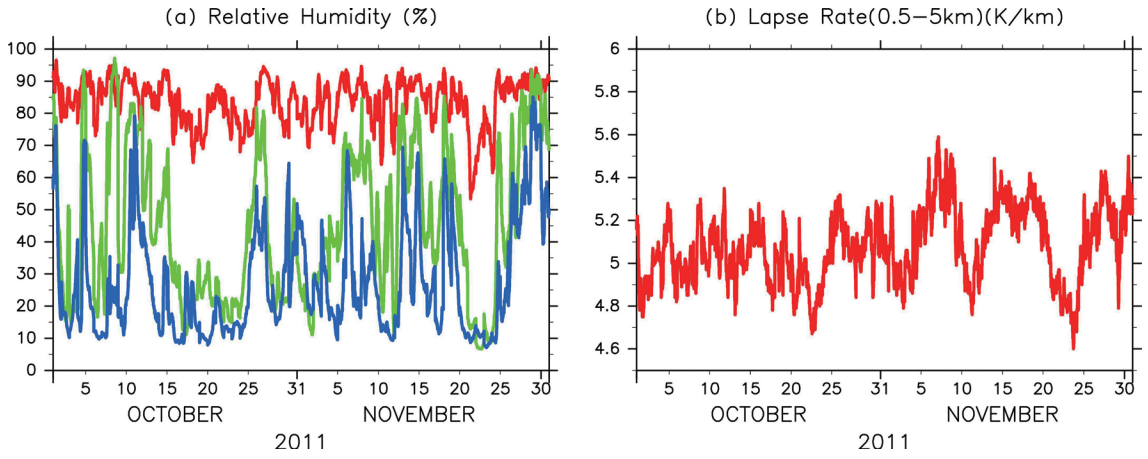

Fig. 6. Time series of (a) mean relative humidity averaged over the Domain 4 area and over the depth of 0–2 km (red line), 2–6 km (green line), and 6–10 km (blue line) and (b) mean temperature lapse rate between the levels of 0.5 and 5 km averaged over Domain 4 from 0000 UTC 1 October to 0000 UTC 1 December 2011.

Stability conditions examined here are evaluated in Domain 4.

Figure 6 shows the time series of mean relative humidity averaged at the low (0–2 km), middle (2–6 km), and upper (6–10 km) levels and temperature lapse rate in the lower troposphere, i.e., the levels between 0.5 and 5 km. The lapse rate in the lower troposphere is examined because of its contribution to cumulus convection development (Takemi 2007a, b, 2010). Consistent with the features found in Fig. 3, low-level relative humidity is basically quite high, fluctuating 80 %–90 %, except for the very dry period before MJO development in late November, while the middle- and upper-level relative humidity largely varies between October and November. The occurrence of high relative humidity is less frequent in the upper levels than in the middle levels. During the development of the November MJO, the relative humidity at the middle as well as upper levels is very high in late November, i.e., after 25 November. It is seen that there are some periods with high relative humidity at the middle and the upper levels, which correspond to higher values of the temperature lapse rate. Higher lapse rate means that the lower troposphere becomes less stable, which will promote convection. The correlation coefficients of the time series of the temperature lapse rate with those of relative humidity in the three layers are 0.30 for the low-level relative humidity, 0.60 for the middle-level relative humidity, and 0.45 for the upper-level relative humidity, which indicates that higher lapse rate does not occur simultaneously in periods with moister conditions. Furthermore, the lapse rate during the development of the two MJO events in late October and late November does not necessarily seem to be the highest during the period shown in Fig. 6. In fact, the highest lapse rate appears in early November when relative humidity becomes high up to the middle levels. With these stability characteristics, we examine cumulus convection activity.

To gain overall views on the simulated cloud activity in Domain 4, we then examine cloud cover computed at each height. The cloud here is defined as grid points having total condensate (i.e., the sum of rainwater, cloud water, cloud ice, snow, and graupel) mixing ratio ≥ 0.01 g kg^{-1}, and the cloud cover is a fractional area of the cloud grids against the total area of Domain 4.

Figure 7 shows the temporal and height variation of cloud cover. At the lower levels below the 3 km height, higher cloud cover, which corresponds to shallow cumulus clouds, is a normal condition for the analysis region with some exceptions of extremely dry situations as seen before the active phase of the MJO events in late October and late November. On the other hand, at the levels above the 3 km height, conditions with higher cloud cover appear less frequently. In particular, higher cloud cover at the middle levels between 3 and 6 km heights is found sporadically but clearly identified in early October, the MJO event in late October, in early November, and the MJO event in late November. In addition, these four time periods indicate higher cloud cover at upper levels above the 6 km height seen on 7–10

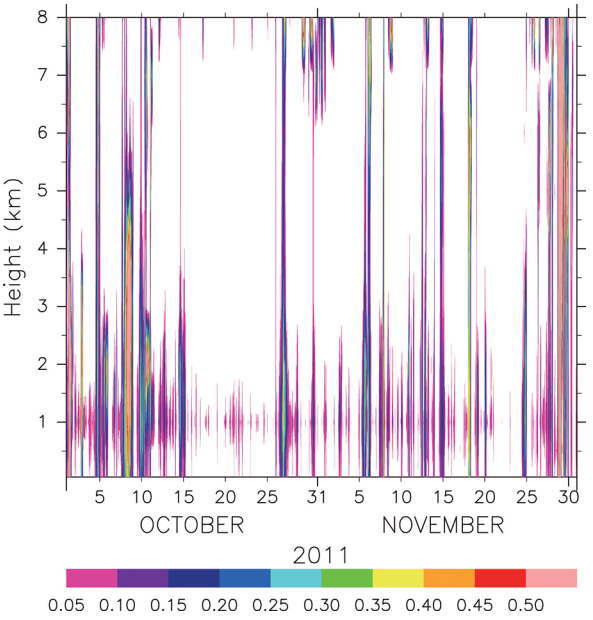

Fig. 7. Time and height diagram of cloud cover simulated in Domain 4 from 0000 UTC 1 October to 0000 UTC 1 December 2011.

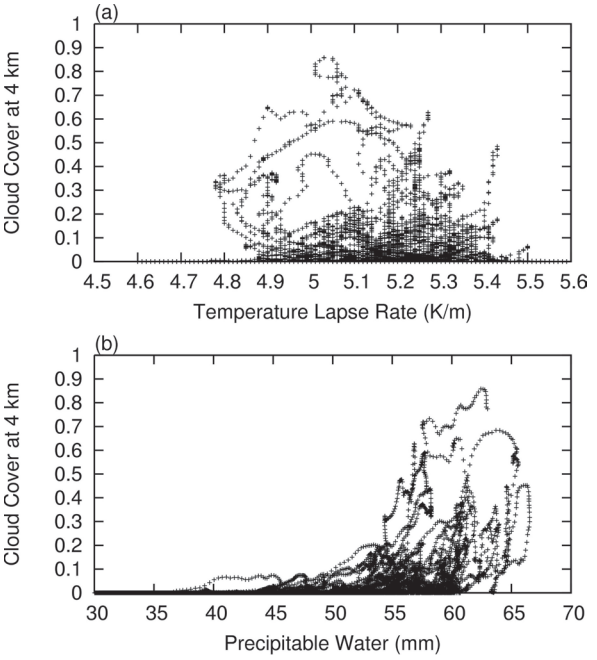

Fig. 8. Relationship of the cloud cover evaluated at the 4 km height in Domain 4 to (a) mean lower tropospheric temperature lapse rate and (b) mean precipitable water vapor averaged over Domain 4. The temperature lapse rate is calculated as in Fig. 6b.

October, 25–26 October, 5–8 November, and 25 November to 1 December.

Based on the analyses shown in Figs. 6 and 7, the relationship between the cloud cover and environmental stability is examined. Because higher cloud cover at levels above the 3 km height shown in Fig. 7 is considered to occur in response to changes in environmental stability, the cloud cover at the 4 km height is chosen. Figure 8 shows the relationship between the cloud cover at the 4 km height and the environmental parameters. It is seen that there is no organized features in Fig. 8a, whereas a distinct relationship is seen in Fig. 8b. It is also seen that the cloud cover significantly increases as precipitable water vapor becomes larger than about 55 mm. This suggests that there is a threshold in precipitable water vapor for cloud development.

From Fig. 8, it was shown that cloud cover at least at the middle levels has a closer relationship with moisture content than temperature lapse rate. Thus, the relationship of the cloud cover to moisture is further investigated. The cloud cover evaluated at a certain height is compared with relative humidity in a lower layer. The idea here is that cumulus clouds will develop vertically with moistening the atmosphere from the low levels to upper levels (Takemi et al. 2004). Cloud cover at a middle level (an upper level) is evaluated at the 4 km (8 km) height, whereas the relative humidity in a low layer (a middle layer) is calculated by taking averages vertically over the depth of 0–2 (2–6) km and horizontally over Domain 4. Figure 9 shows the relationship between cloud cover at a certain level and a lower layer relative humidity. From Figs. 9a and 9b, it is seen that the cloud cover at the 4 km height sharply increases when the relative humidity in the lower layer exceeds 70 %–80 %. Although the features for the cloud cover at the 8 km height shown in Fig. 9c seem less clear, there is an increasing tendency of the upper-level cloud cover with the increase in the relative humidity in the middle layer. In Fig. 9c, a higher value in the cloud cover is found for some cases with lower values of the relative humidity; higher cloud cover over 0.3 can be seen in cases of relative humidity < 40 %. This corresponds to upper-level clouds not rooted in the lower levels as seen above the 7 km height in Fig. 7, which may be horizontally advected. By excluding these cases of higher cloud cover in drier conditions, we can clearly identify a positive relationship between the upper-level cloud cover and the middle layer relative

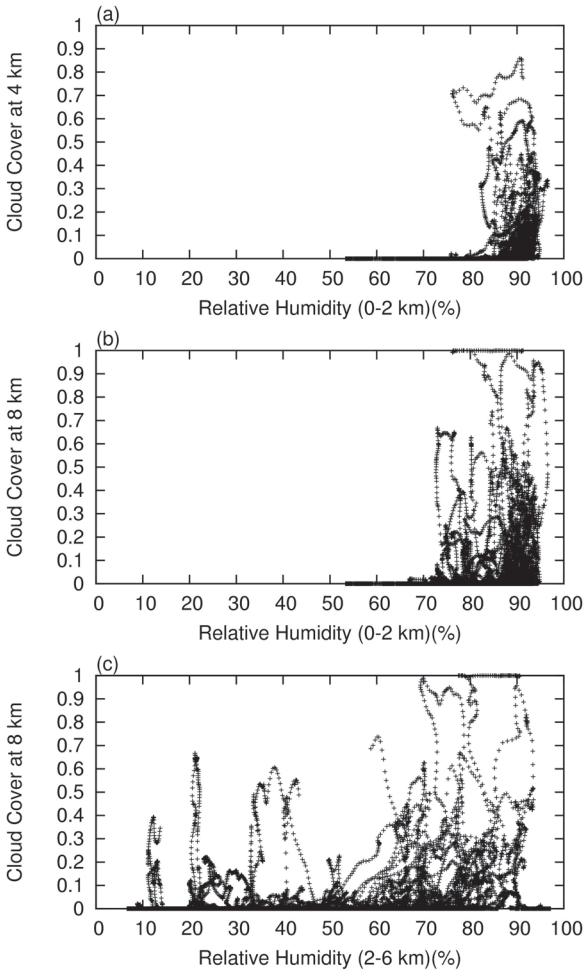

Fig. 9. Relationship between cloud cover and relative humidity: (a) for the cloud cover at the 4 km height and the mean low-level relative humidity averaged in Domain 4, (b) for the cloud cover at the 8 km height and the mean low-level relative humidity in Domain 4, and (c) for the cloud cover at the 8 km height and the mean middle-level relative humidity in Domain 4.

humidity.

The development of cumulus convection is diagnosed by updraft intensity. As described in Section 1, the updraft velocity in tropical cumulus convection is significantly smaller than that in the mid-latitude counterpart. Typically, the updraft velocity in tropical cumulus clouds is a few m s^{-1}. For example, Zipser and LeMone (1980) and LeMone and Zipser (1980) estimated, from the analysis of observational data, that the median updraft within the region of stronger upward motion in tropical cumulus clouds, i.e., updraft core, is about 2 m s^{-1}, and Igau et al. (1999) obtained the value of 2.25 m s^{-1} as the average speed of updraft cores. LeMone and Zipser (1980) and Jorgensen and LeMone (1989) defined the threshold speed for updraft as being 0.5 m s^{-1} and that for updraft core as being 1 m s^{-1}, and Jorgensen and LeMone (1989) and Igau et al. (1999) used the same threshold for identifying updraft cores. By considering the definitions used in these previous studies, we define cloud core as having total water condensate mixing ratio $\geq$ 0.01 g kg^{-1} and updraft speed $\geq$ 0.5 m s^{-1}. This threshold value for the updraft speed, which is smaller than that used in the observational analyses, is chosen because the simulated flow speed is generally weaker than the observed instantaneous wind speed. We determine a grid point with these properties as a cloud-core grid. With this procedure, the mean updraft velocity averaged for cloud-core grids is evaluated at each height.

Figure 10 shows the temporal variation of the mean updraft velocity in cloud cores. Stronger updrafts > 2.5 m s^{-1} are occasionally seen at levels above the 3 km height, corresponding to the increased cloud cover at the middle and upper levels, as indicated in Fig. 7. The updraft velocity peak is found at 5 to 6 km heights. These signatures of stronger updraft > 3 m s^{-1} are the manifestation of deep convection development. During the MJO event in late November, persistent stronger updrafts at middle-to-upper levels appear, following suppressed updrafts within the lowest 2 km depth.

The characteristics of updraft in late November are considered to reflect the cumulus activity during the MJO event in the period. Thus, we now focus on the environmental conditions in late November.

The temporal variation of temperature lapse rate in the lower troposphere, i.e., the levels between 0.5 and 5 km and relative humidity over the depths of 0–2 km (low levels) and 2–6 km (middle levels) from 0000 UTC 21 November to 0000 UTC 1 December are shown in Fig. 11. From 21 to 23 November, the temperature lapse rate is very low, and the relative humidity at the middle levels is also very low. The low-level relative humidity is also lower than the temporal average during the two months, i.e., 83.5 % (Fig. 6a), indicating that the atmosphere is very stable and dry. After 24 November, the temperature lapse rate gradually increases, and the low-level relative humidity recovers the normal values. In addition, the middle-level relative humidity also increases day by day: three diurnal cycles of the increase in the middle-level relative humidity are seen during 24 and

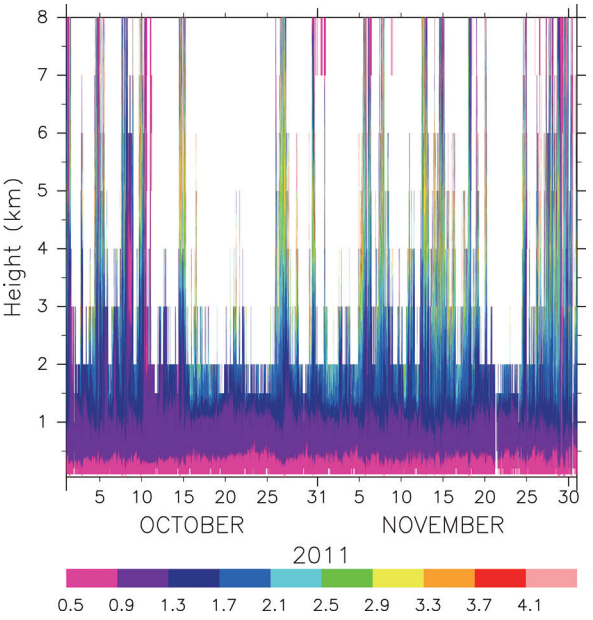

Fig. 10. Time and height diagram of mean updraft velocity (in m s^{-1}) averaged for cloud-core grids from 0000 UTC 1 October to 0000 UTC 1 December 2011.

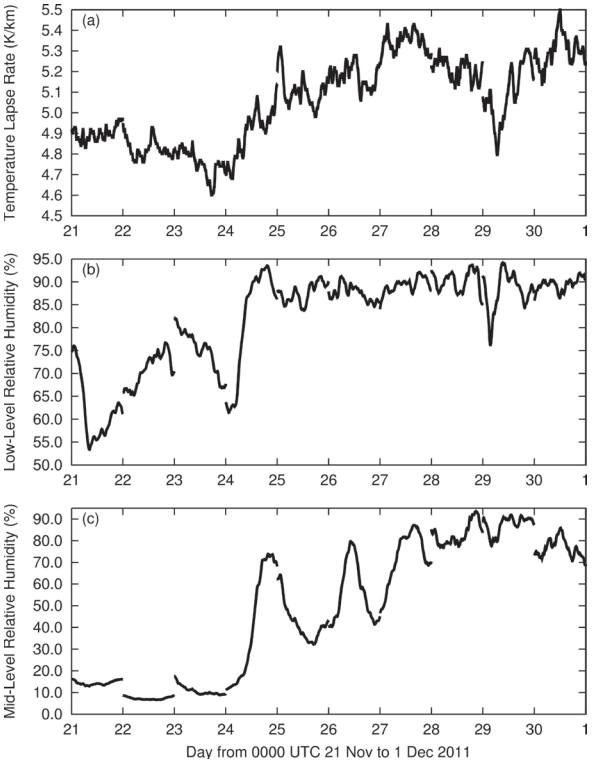

Fig. 11. Time series of (a) mean temperature lapse rate in the lower troposphere, (b) low-level relative humidity, and (c) middle-level relative humidity averaged over Domain 4 from 0000 UTC 21 November to 0000 UTC 1 December 2011.

27 November. After this cycle of the relative humidity increases, the atmosphere becomes more unstable and moister not only at the low levels but also at the middle levels. The middle-level relative humidity after 27 November is significantly higher than the two-month mean value of 45.0 %.

The temporal variation of such instability and moisture conditions can also be clearly identified by other parameters. Figure 12 demonstrates the temporal variation of precipitable water vapor and convective available potential energy (CAPE) during the same period as in Fig. 11. CAPE was computed by raising an air parcel at the 100 m height above the ocean surface. From 21 to 23 November, precipitable water vapor is significantly low, and CAPE is virtually zero. On 24 November, the moisture content and instability increases. After three days, the moisture content becomes larger than 60 mm, and CAPE exceeds 1000 J kg^{-1}. With these increases, higher cloud cover with stronger updrafts develops, as indicated in Figs. 7 and 10.

The analyses presented in this section clearly indicate that the increases in cloud cover, updraft intensity, and even the depth of cloud have a close correlation with the increase in relative humidity at the middle-to-upper levels. From this, it is further suggested that there would be interacting processes between cumulus activity and environmental moisture. The next section will discuss this issue.

3.3 *Role of cumulus convection in environmental moistening*

In the present simulations, the computational domains are set with one-way nesting. This means that there is no feedback from an inner domain to an outer domain. In other words, the averaged states simulated in an inner domain will differ from those in an outer domain. Thus, by comparing the results simulated in an inner domain and an outer domain, we can diagnose the effects of explicitly resolved processes in a higher-resolution domain on the atmospheric states. In this section, we examine possible roles of cumulus convection sufficiently resolved in Domain 4 in determining the atmospheric conditions of the background fields. For this purpose, we compare the results obtained in Domain 4 with those

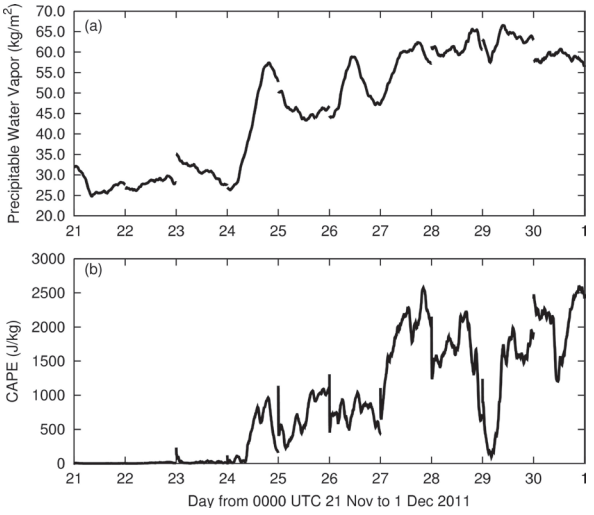

Fig. 12. The same as Fig. 11, except for (a) precipitable water vapor and (b) CAPE averaged over Domain 4.

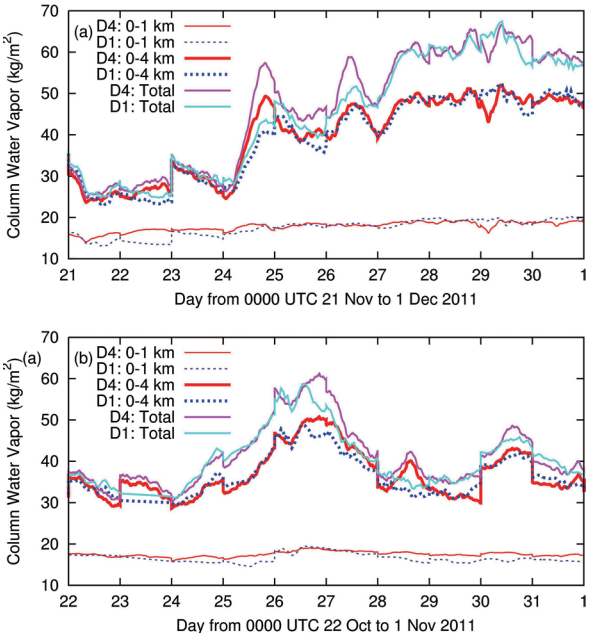

Fig. 13. Time series of mean column water vapor content averaged over the area corresponding to Domain 4 (a) from 0000 UTC 21 November to 0000 UTC 1 December 2011 and (b) from 0000 UTC 22 October to 0000 UTC 1 November 2011. Thin solid red line and thin dotted blue line indicate the column water vapor content at 0–1 km obtained from the Domain 4 and Domain 1 results, respectively. Thick solid red line and thick dotted blue line indicate the column content at 0–4 km obtained from Domains 4 and 1, respectively. Solid purple line and solid light blue line indicate the total content (i.e., precipitable water vapor) obtained from Domains 4 and 1, respectively.

in Domain 1.

From the previous section, it was indicated that cloud development has a close relationship with moisture variation. Therefore, we examine the differences in moisture content simulated in Domains 4 and 1. The simulated results of Domains 4 and 1 are compared in terms of mean column water vapor content within a certain depth averaged over the area corresponding to the Domain 4 region.

Figure 13a compares the mean column water vapor contents in the lowest 1 km depth, in the lowest 4 km depth, and in the entire troposphere simulated in Domains 4 and 1 from 0000 UTC 21 November to 0000 UTC 1 December 2011. From 21 to 24 November, there is a prominent difference in the column water vapor in the 0–1 km layer between the results of Domains 4 and 1: the moisture content of the Domain 4 simulation is larger than that of the Domain 1 simulation. Larger moisture content in Domain 4 than in Domain 1 can also be seen for the moisture content in the 0–4 km layer during the first half of the period, as shown in Fig. 13a. In particular, on 24 November, the moisture content in the 0–4 km layer is much larger in the Domain 4 case than in the Domain 1 case. This difference corresponds to the sharp increase in middle-level relative humidity identified in Fig. 11c, and it significantly influences the difference in the total moisture content between the Domain 4 and 1 cases. Larger value of the total moisture content in the Domain 4 case is seen to continue for three days starting at 24 November, while the moisture content in the lowest 1 km depth after 24 November is similar with each other in the Domain 4 and 1 cases. Therefore, it is strongly suggested that the larger moisture content in the Domain 4 case than in Domain 1 is due to more increased moisture at middle-to-upper levels in Domain 4 than in Domain 1, which will promote deep convection, as shown in the cloud cover (Fig. 7) and in the updraft intensity (Fig. 10).

The differences in the moisture contents in Domains 4 and 1 are also examined for the other MJO case in late October. As in Fig. 13a, Fig. 13b exhibits the temporal changes in the moisture contents from 0000 UTC 22 October to 0000 UTC

1 November 2011. We here focus on the time period of the increasing tendency of moisture from 23 to 26 October. Higher moisture contents at the lowest layer between the heights of 0 and 1 km in Domain 4 than in Domain 1 can be seen from 23 to 25 October. In addition, higher moisture contents in Domain 4 than in Domain 1 can be identified at the layer extending to the middle levels occasionally from 23 to 26 October. Owing to these higher moisture conditions in Domain 4, the total moisture contents become higher in Domain 4 than in Domain 1. Therefore, the characteristics of the moisture conditions in the highest resolution domain as seen in the November MJO event can also be identified in the October MJO event.

To diagnose the effects of cumulus convection on the environmental atmosphere, we use thermodynamic conserved variables to examine a possible role of cumulus convection. Equivalent potential temperature (as computed by the analytic equations of Bolton (1980)) and total water mixing ratio, which is the sum of water vapor and water condensate, are used for this diagnosis. Data outputs from all the Domain 4 simulations from 0000 UTC 1 October to 0000 UTC 1 December in 2011 are analyzed. We categorize all the grid points in Domain 4 into a cloud-core parcel, a cloud parcel (but not cloud core), and an environmental parcel. The definitions of the cloud core and the cloud are the same, as described in Section 3.2. Equivalent potential temperature and total water mixing ratio at all the grid points are then computed. After determining the properties of grid points, the values of each thermodynamic variable at those grids are averaged for each category of cloud core, cloud, and environment at each height.

The thermodynamic properties averaged for each category of air parcels at the heights of 100, 1000, 2000, 4000, and 6000 m are indicated in Fig. 14. Air parcels at lower heights have higher equivalent potential temperature and larger total water mixing ratio. Red, blue, and green points at each height in this thermodynamic space are clustered on a line declining toward the right. At the height of 100 m, the differences among the parcel categories seem to be small, which means that there would be no clear distinction among the thermodynamic properties of the parcel categories, and therefore, the air parcels are well mixed. The differences among the parcel categories at the upper levels above the 1000 m height become quite pronounced, which means that the thermodynamic properties are quite different between cloudy and environmental parcels. There is also a clear distinction between the cloud core and cloud parcels:

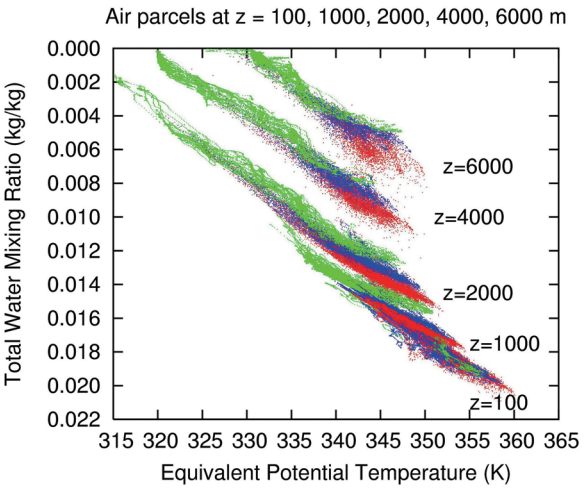

Fig. 14. Scatter plot of parcel properties at the heights of 100 m, 1000 m, 2000 m, 4000 m, and 6000 m in a conserved variable space by equivalent potential temperature and total water (i.e., the sum of condensate and vapor) mixing ratio. Red, blue, and green dots denote the cloud-core parcels, cloud parcels, and environmental parcels. The simulated outputs of Domain 4 at all the output time steps from 0000 UTC 1 October to 0000 UTC 1 December 2011 are used.

the cloud-core parcels have a higher value of equivalent potential temperature and a larger amount of total water than the cloud parcels. The distributions of the parcels' properties at each height indicate that the thermodynamic properties of the cloud parcels are closer to those of the environmental parcels and that the properties of the cloud-core parcels have a distinct feature from other categories. Furthermore, the equivalent potential temperature of the cloud-core parcels does not change much in the vertical in comparison to that of the cloud parcels. Therefore, it is considered that the cloud-core parcels are less affected by mixing with the environment than the cloud parcels. This suggests that cloud-core parcels would be undiluted during the ascent in the vertical.

As described in Section 1, the updraft intensity is weaker in tropical convective clouds than in the mid-latitude ones. In addition, the size of the updraft core regions within convective clouds is usually smaller in the tropics than in the mid-latitude (LeMone and Zipser 1980; Zipser and LeMone 1980). Weaker updraft, which is due to smaller buoyancy (Lucas et al. 1994a), and smaller area of updraft cores in tropical convection lead to unfavorable effects

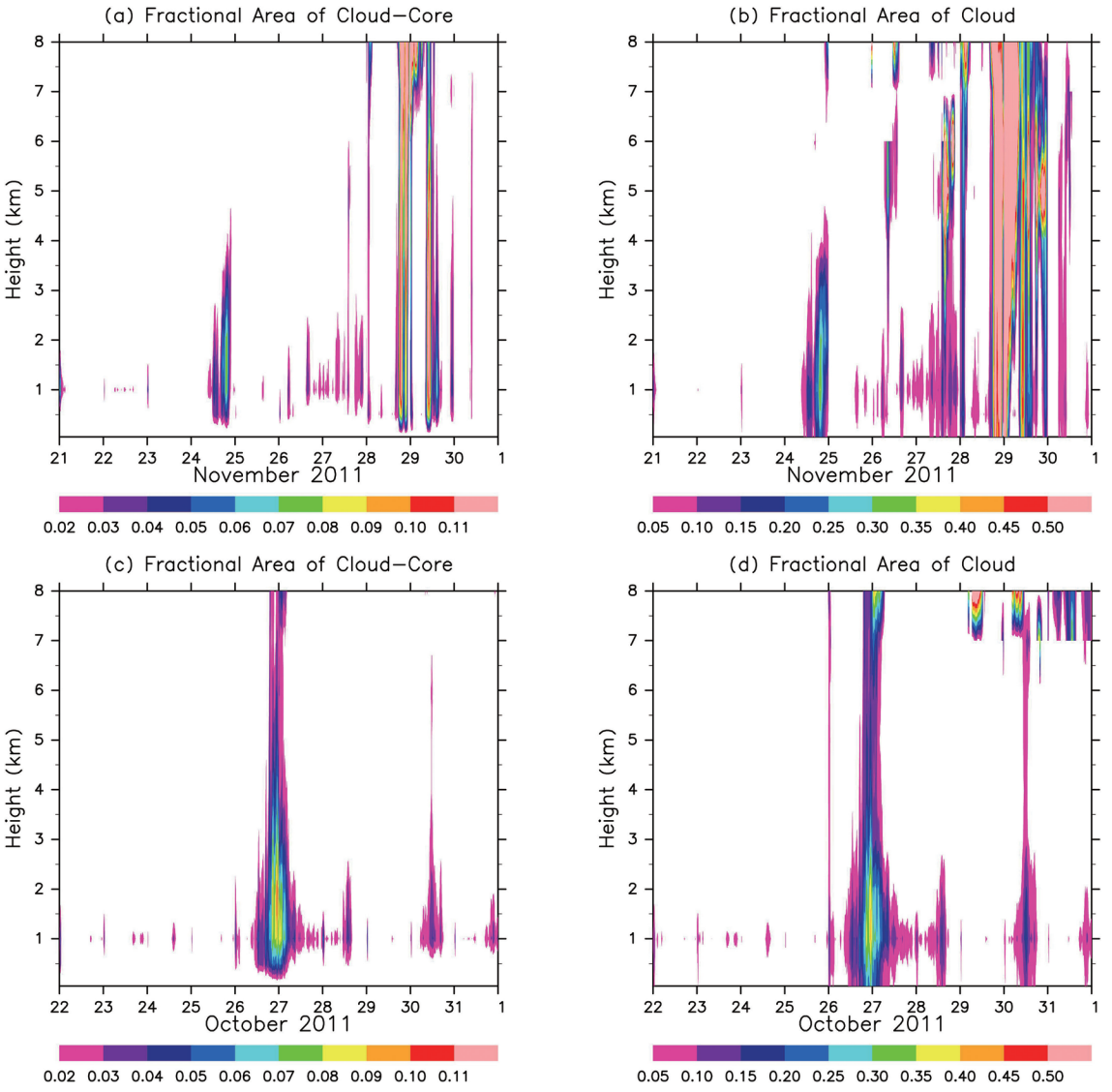

Fig. 15. Time and height diagram of (a) the fractional area of the cloud-core parcels and (b) the fractional area of the cloud parcels in Domain 4 from 0000 UTC 21 November to 0000 UTC 1 December 2011, (c) the fractional area of the cloud-core parcels, and (d) the fractional area of the cloud parcels in Domain 4 from 0000 UTC 22 October to 0000 UTC 1 November 2011.

for cumulus development in which updraft cores are susceptible to dilution with the environment. In other words, larger areas of updraft cores will lead to the vertical development of cumulus clouds in the tropics (Feng et al. 2015). Because of the importance of the size of the updraft area, the areal coverages of the cloud-core parcels and cloud parcels are examined here. We examine the fractional areas of the cloud core and the cloud coverage against the Domain 4 area as a proxy for the size of the updraft.

The temporal changes of the fractional coverages of the cloud-core parcels and the cloud parcels at each height within the Domain 4 area for the November MJO case (from 21 November to 1 December) and for the October MJO case (from 22 October to 1 November) are demonstrated in Fig. 15. In the November case, the increase in the fractional coverage seems to occur simultaneously on 24 November, and the increase in the fractional coverage of the cloud parcels precedes that in the fractional

area of the cloud-core parcels. Although the signatures seen in this November case appear to be less clear in the October case, the increase in the fractional coverage of the cloud-core parcels occurs with the increase in the coverage of the cloud parcels during the October event.

The upward penetration of the cloud-core parcels will transport sufficient amount of water to form cumulus clouds, which will moisten the environmental atmosphere. Higher values of the moisture content simulated in Domain 4 than those in Domain 1, as shown in Fig. 13, strongly supports the role of cumulus clouds in moistening the environment. The larger areas of the cloud cores will be beneficial for the upward penetration of convective updraft.

4. Discussion

By conducting convection-resolving simulations of the Indian Ocean tropical convection in which the higher computational domains are nested in one way, we have indicated that the simulated fields in Domain 4 are more moistened than those in Domain 1 during the two major MJO periods. From the analyses of updraft and cloud properties, it is strongly suggested that widespread cloud-core parcels penetrate upward without being less affected by mixing with the environmental air. These less diluted cloud-core parcels are considered to contribute to the moistening of the environmental atmosphere. In the study of Takemi et al. (2004), it was shown that the control of the vertical development of cumulus clouds is due to the environmental humidity: higher humidity at middle levels leads to the development of taller cumulus clouds. In this study, we have indicated that there is an upscale influence from the activity of cumulus clouds to their environmental atmosphere.

One of the issues to remain unsolved is the relative role of the atmospheric moistening from cumulus clouds against the synoptic-scale variability of the atmospheric humidity. In this study, we have not evaluated the roles of cumulus clouds and synoptic-scale variability on moistening the atmosphere. By examining reanalysis and satellite data during the CINDY2011/DYNAMO period, Nasuno et al. (2015) demonstrated that the zonal advection of low frequency moisture, which has a maximum over the Maritime Continent, by intra-seasonal easterly anomalies and advection of intra-seasonal moisture by the basic zonal wind account for the atmospheric moistening during the preconditioning periods of the October and November MJO events. Once the MJO-scale convective envelope is established, moistening by vertical advection occurs. Based on their study, a certain level of the humidification of the atmosphere seems to be required for initiating active convection during the MJO events. Considering that middle-level moist conditions promote the vertical development of cumulus clouds (Takemi et al. 2004), the humidification of the environmental atmosphere enhances the cumulus development, and hence the moistening due to cumulus activity. From Figs. 8b and 9, it seems that there are some moisture thresholds for convection development. It is well documented from observations that there is a non-linear relationship between precipitation and precipitable water vapor in the tropics: precipitation increases sharply with precipitable water vapor above a certain critical value (Bretherton et al. 2004; Holloway and Neelin 2009, 2010). This observational evidence supports the present results indicating the threshold values of moisture content for convection development.

The threshold indicated from Figs. 8 and 9 is considered to be partly controlled by large-scale atmospheric variability like the one shown in the study of Nasuno et al. (2015). It is further suggested that the moistening processes may be different for the active and suppressed phase of MJO because the base-state atmospheric conditions such as stability and moisture are quite different between the two phases. From the analyses of observed data obtained during DYNAMO, Ruppert and Johnson (2015) indicated that the humidification of the low-to-middle troposphere is due to simultaneous changes in convective cloud population as well as large-scale circulation and that the diurnal cycle of convective clouds plays a role in the moistening of the troposphere. The results of the present simulations are consistent with the findings of Ruppert and Johnson (2015).

Another issue to be solved is the triggering processes for cumulus clouds. Feng et al. (2015) suggested that closely spaced, large clouds moisten the surrounding environment and reduce entrainment drying, which contribute to increase the probability of the organization of deep convection. The convective clouds are triggered by surface cold pools. From the analyses of the data obtained by the 2011 Atmospheric Radiation Measurement (ARM) MJO Investigation Experiment (AMIE)/DYNAMO field campaign, cold pools generated by convective clouds were commonly observed to interact, which serves as a triggering mechanism for the convective development. The existence of prevalent cold pools were identified from the observations in a tropical oceanic region (Zuidema et al. 2011), and the importance of

cold pools for the organization of tropical convection was numerically investigated by Tompkins (2001). Further analyses are required to identify the triggering mechanisms for developing convection and the resulting moisture transport due to convective updrafts.

5. Summary and conclusions

This study investigated the relationship between cumulus convection activity and environmental moisture variation in the tropical Indian Ocean during October and November 2011 with the use of the WRF model at a convection-resolving resolution, i.e., the horizontal grid spacing of 100 m. By setting four computational domains with the nesting capability of the WRF model, the outermost computational domain had an area of 4250 km × 3000 km, which covered most of the tropical Indian Ocean, while the innermost domain, having the 100 m resolution, covered a mesoscale domain of 100 km × 60 km centered at the stationary observation point (80.5°E and 8°S) of the R/V Mirai as a part of the CINDY2011/DYNAMO field experiment. By performing two-day segmented simulations with a suite of full physics processes, the simulated data were obtained from 0000 UTC 1 October 2011 to 0000 UTC 1 December 2011 with the background fields kept consistent with the global analysis data of JMA. The data outputs in the mesoscale region were mainly used to examine cumulus activity and environmental variability over the region.

The results obtained in the simulations in the outermost computational domain indicated that eastward propagating signals corresponding to MJOs in the Indian Ocean in late October and late November were successfully reproduced. The temporal variations of the tropospheric moisture observed by radiosondes at the stationary point of the R/V Mirai were also well captured in the simulations in the innermost computational domain. By demonstrating the favorable performance of the simulated results compared with the observed features, we examined the relationship between cumulus activity and environmental variability from the high-frequency (i.e., the 5 min interval) data outputs in the innermost domain. Our philosophy to conduct convection-resolving simulations at the 100 m resolution is that the processes relevant to cumulus clouds are expected to be sufficiently resolved (Bryan et al. 2003), and therefore, the analyses on cumulus activity and its inter-relationship with the environment should be robust. The large-scale atmospheric variations, such as two MJOs successfully simulated in the outermost domain, were regarded as a prescribed background condition for the innermost domain.

From the examination of domain-averaged temperature and moisture properties simulated in the innermost domain, it was indicated that relative humidity at the middle and upper levels largely vary during October and November 2011. The moister conditions at middle-to-upper levels in some cases correspond to higher temperature lapse rates; however, the moister periods corresponding to the MJO events does not necessarily mean that the temperature lapse rate demonstrates the most unstable condition at the same time. The examination of cloud cover at a middle level of 4 km indicated that the cloud cover has a closer relationship with precipitable water vapor than temperature lapse rate in the lower troposphere. It was also shown that the cloud cover sharply increases with the increase in precipitable water vapor exceeding about 55 mm. This value can be regarded as a threshold for developing clouds in the vertical above the middle level.

From the comparison of cloud cover at a certain level with relative humidity in a lower layer, it was indicated that the cloud cover at a middle level of 4 km sharply increases with the increase in relative humidity in the lower layer and that the cloud cover at an upper level of 8 km also increases with the relative humidity increase in the lower layer. In other words, the increase in relative humidity in a lower layer results in the increase in cloud cover at a level above the moist layer.

Corresponding to the periods with higher cloud cover, updrafts within cloud-core areas, that is, proxy for the development of cumulus convection, are intensified at middle and upper levels. In particular, persistent updrafts at middle-to-upper levels are seen during the MJO event in late November.

Because the present regional simulations were conducted with one-way nesting, the results obtained from the outermost and innermost domains may differ with each other. Therefore, from the comparison of the simulated results in the outermost and innermost domains, the effects of explicitly resolved cumulus clouds on the background condition can be diagnosed. This analysis was conducted for the time periods of late October and November, corresponding to the October and late November MJOs in the CINDY2011/DYNAMO campaign. The comparison in terms of moisture variables showed that the moisture content in the middle levels is significantly larger in the innermost domain than in the outermost domain, suggesting that the effects of cumulus clouds

play a role.

The analysis with the use of thermodynamically conserved variables demonstrated that the cloud-core parcels have a distinct feature from the parcels in the clouds but outside core and the environments. It is considered that the cloud-core parcels are less affected by being mixed with the environment than cloud parcels outside the core areas. This suggests that the cloud-core parcels are less susceptible to the negative effects of dilution with the environmental air and survive to penetrate to higher levels. Those core parcels will transport water vapor from the lower levels to middle-to-upper levels to form cumulus clouds and induce the moistening of the environmental atmosphere.

From the convection-resolving simulations with the horizontal grid spacing of 100 m, the relationship between cumulus activity and environmental conditions is clearly revealed. The existence of widespread updraft cores that are less diluted with the environment plays a key role in an inter-relationship between cumulus clouds and their environment: the moisture condition controls the vertical development of cumulus clouds, whereas the development of cumulus clouds provide moistening effects on the environmental atmosphere. The effects from cumulus clouds on their environment obtained from the present simulations are regarded as a preconditioning influence for the convective initiation of MJO. The moisture variability at cumulus scales should be considered for the understanding the convective initiation of MJO.

Acknowledgments

I would like to thank Dr. Kunio Yoneyama at JAMSTEC for giving us the opportunity to participate in the radiosonde observation on board the R/V Mirai during the cruise MR11-07 Leg-1 in October 2011 as a part of the field campaign of the CINDY/DYNAMO program. I would also like to thank Ms. Nao Takamura and Aya Tsuboi, who were former graduate students of Kyoto University and were on board the R/V Mirai during the MR11-07 Leg-1 cruise, for obtaining radiosonde data. The comments by the two anonymous reviewers are greatly acknowledged in improving the original manuscript. This study was supported by the grant under Strategic Programs for Innovative Research (SPIRE)-Field 3 “Projection of Planet Earth Variations for Mitigating Natural Disasters” and also partly supported by a Scientific Research grant from Japan Society for Promotion of Sciences (JSPS). The GFD Dennou Library was used for drawing some of the figures.

References

Bolton, D., 1980: The computation of equivalent potential temperature. *Mon. Wea. Rev.*, **108**, 1046–1053.

Bretherton, C. S., M. E. Peters, and L. E. Back, 2004: Relationships between water vapor path and precipitation over the tropical oceans. *J. Climate*, **17**, 1517–1528.

Brown, R. G., and C. Zhang, 1997: Variability of midtropospheric moisture and its effect on cloud-top height distribution during TOGA COARE. *J. Atmos. Sci.*, **54**, 2760–2774.

Bryan, G. H., J. C. Wyngaard, and J. M. Fritsch, 2003: Resolution requirements for the simulation of deep moist convection. *Mon. Wea. Rev.*, **131**, 2394–2416.

Ciesielski, P. E., H. Yu, R. H. Johnson, K. Yoneyama, M. Katsumata, C. N. Long, J. Wang, S. M. Loehrer, K. Young, S. F. Williams, W. Brown, J. Braun, and T. Van Hove, 2014: Quality-controlled upper-air sounding dataset for DYNAMO/CINDY/AMIE: Development and corrections. *J. Atmos. Oceanic Technol.*, **31**, 741–764.

Deardorff, J. W., 1980: Stratocumulus-capped mixed layers derived from a three-dimensional model. *Bound.-Layer Meteor.*, **18**, 495–527.

Del Genio, A. D., Y. Chen, D. Kim, and M.-S. Yao, 2012: The MJO transition from shallow to deep convection in CloudSat/CALIPSO data and GISS GCM simulations. *J. Climate*, **25**, 3755–3770.

Derbyshire, S. H., I. Beau, P. Bechtold, J.-Y. Grandpeix, J.-M. Piriou, J.-L. Redelsperger, and P. M. M. Soares, 2004: Sensitivity of moist convection to environmental humidity. *Quart. J. Roy. Meteor. Soc.*, **130**, 3055–3079.

Dudhia, J., 1989: Numerical study of convection observed during the winter monsoon experiment using a mesoscale two-dimensional model. *J. Atmos. Sci.*, **46**, 3077–3107.

Feng, Z., S. Hagos, A. K. Rowe, C. D. Burleyson, M. N. Martini, and S. P. de Szoeke, 2015: Mechanisms of convective cloud organization by cold pools over tropical warm ocean during the AMIE/DYNAMO field campaign. *J. Adv. Model. Earth Syst.*, **7**, 357–381.

Fu, X., J.-Y. Lee, P.-C. Hsu, H. Taniguchi, B. Wang, W. Wang, and S. Weaver, 2013: Multi-model MJO forecasting during DYNAMO/CINDY period. *Climate Dyn.*, **41**, 1067–1081.

Gottschalck, J., P. E. Roundy, C. J. Schreck III, A. Vintzileos, and C. Zhang, 2013: Large-scale atmospheric and oceanic conditions during the 2011–2012 DYNAMO field campaign. *Mon. Wea. Rev.*, **141**, 4173–4196.

Hagos, S., Z. Feng, S. McFarlane, and L. R. Leung, 2013: Environment and the lifetime of tropical deep convection in a cloud-permitting regional model simulation. *J. Atmos. Sci.*, **70**, 2409–2425.

Hagos, S., Z. Feng, K. Landu, and C. N. Long, 2014: Advection, moistening, and shallow-to-deep convection transitions during the initiation and propagation of Madden-Julian Oscillation. *J. Adv. Model. Earth Syst.*, **6**, 938–949.

Hohenegger, C., and B. Stevens, 2013: Preconditioning deep convection with cumulus congestus. *J. Atmos. Sci.*, **70**, 448–464.

Holloway, C. E., and J. D. Neelin, 2009: Moisture vertical structure, column water vapor, and tropical deep convection. *J. Atmos. Sci.*, **66**, 1665–1683.

Holloway, C. E., and J. D. Neelin, 2010: Temporal relations of column water vapor and tropical precipitation. *J. Atmos. Sci.*, **67**, 1091–1105.

Holloway, C. E., S. J. Woolnough, and G. M. S. Lister, 2013: The effects of explicit versus parameterized convection on the MJO in a large-domain high-resolution tropical case study. Part I: Characterization of large-scale organization and propagation. *J. Atmos. Sci.*, **70**, 1342–1369.

Hong, S.-Y., and J.-O. J. Lim, 2006: The WRF single-moment 6-class microphysics scheme (WSM6). *J. Korean Meteor. Soc.*, **42**, 129–151.

Hong, S.-Y., Y. Noh, and J. Dudhia, 2006: A new vertical diffusion package with an explicit treatment of entrainment processes. *Mon. Wea. Rev.*, **134**, 2318–2341.

Igau, R. C., M. A. LeMone, and D. Wei, 1999: Updraft and downdraft cores in TOGA COARE: Why so many buoyant downdraft cores? *J. Atmos. Sci.*, **56**, 2232–2245.

Jensen, M. P., and A. D. Del Genio, 2006: Factors limiting convective cloud-top height at the ARM Nauru Island climate research facility. *J. Climate*, **19**, 2105–2117.

Johnson, R. H., and P. E. Ciesielski, 2013: Structure and properties of Madden-Julian oscillations deduced from DYNAMO sounding arrays. *J. Atmos. Sci.*, **70**, 3157–3179.

Johnson, R. H., T. M. Rickenbach, S. A. Rutledge, P. E. Ciesielski, and W. H. Schubert, 1999: Trimodal characteristics of tropical convection. *J. Climate*, **12**, 2397–2418.

Jorgensen, D. P., and M. A. LeMone, 1989: Vertical velocity characteristics of oceanic convection. *J. Atmos. Sci.*, **46**, 621–640.

Kumar, V. V., A. Protat, C. Jakob, and P. T. May, 2014: On the atmospheric regulation of the growth of moderate to deep cumulonimbus in a tropical environment. *J. Atmos. Sci.*, **71**, 1105–1120.

LeMone, M. A., and E. J. Zipser, 1980: Cumulonimbus vertical velocity events in GATE. Part I: Diameter, intensity, and mass flux. *J. Atmos. Sci.*, **37**, 2444–2457.

Lucas, C., E. J. Zipser, and M. A. LeMone, 1994a: Vertical velocity in oceanic convection off tropical Australia. *J. Atmos. Sci.*, **51**, 3183–3193.

Lucas, C., E. J. Zipser, and M. A. LeMone, 1994b: Convective available potential energy in the environment of oceanic and continental clouds: Correction and comments. *J. Atmos. Sci.*, **51**, 3829–3830.

Madden, R. A., and P. R. Julian, 1971: Detection of a 40-50-day oscillation in the zonal wind in the tropical Pacific. *J. Atmos. Sci.*, **28**, 702–708.

Madden, R. A., and P. R. Julian, 1972: Description of global-scale circulation cells in the tropics with a 40-50 day period. *J. Atmos. Sci.*, **29**, 1109–1123.

Mlawer, E. J., S. J. Taubman, P. D. Brown, M. J. Iacono, and S. A. Clough, 1997: Radiative transfer for inhomogeneous atmospheres: RRTM, a validated correlated-k model for the long-wave. *J. Geophys. Res.*, **102**, 16663–16682.

Nasuno, T., 2013: Forecast skill of Madden-Julian oscillation events in a global nonhydrostatic model during the CINDY2011/DYNAMO observation period. *SOLA*, **9**, 69–73.

Nasuno, T., T. Li, and K. Kikuchi, 2015: Moistening processes before the convective initiation of Madden–Julian oscillation events during the CINDY2011/DYNAMO period. *Mon. Wea. Rev.*, **143**, 622–643.

Rapp, A. D., C. D. Kummerow, and L. Fowler, 2011: Interactions between warm rain clouds and atmospheric preconditioning for deep convection in the tropics. *J. Geophy. Res.*, **116**, D23210, doi:10.1029/2011JD016143.

Ruppert, J. H., and R. H. Johnson, 2015: Diurnally modulated cumulus moistening in the preonset stage of the Madden-Julian oscillation during DYNAMO. *J. Atmos. Sci.*, **72**, 1622–1647.

Skamarock, W. C., J. B. Klemp, J. Dudhia, D. O. Gill, O. M. Barker, M. G. Duda, X. Y. Huang, W. Wang, and J. G. Powers, 2008: *A description of the advanced research WRF version 3*. NCAR Technical Note, **475**, 113 pp.

Takemi, T., 2007a: A sensitivity of squall line intensity to environmental static stability under various shear and moisture conditions. *Atmos. Res.*, **84**, 374–389.

Takemi, T., 2007b: Environmental stability control of the intensity of squall lines under low-level shear conditions. *J. Geophys. Res.*, **112**, D24110, doi:10.1029/2007JD008793.

Takemi, T., 2008: An eddy-resolving simulation of the diurnal variation of fair-weather convection and tracer transport. *Atmos. Res.*, **89**, 270–282.

Takemi, T., 2010: Dependence of the precipitation intensity in mesoscale convective systems to temperature lapse rate. *Atmos. Res.*, **96**, 273–285.

Takemi, T., 2012: Importance of the numerical representation of shallow and deep convection for simulations of dust transport over a desert region. *Adv. Meteor.*, 413584, doi:10.1155/2012/413584.

Takemi, T., 2014: Convection and precipitation under various stability and shear conditions: Squall lines in tropical versus midlatitude environment. *Atmos. Res.*,

142, 111–123.

Takemi, T., and R. Rotunno, 2003: The effects of subgrid model mixing and numerical filtering in simulations of mesoscale cloud systems. *Mon. Wea. Rev.*, **131**, 2085–2101.

Takemi, T., O. Hirayama, and C. Liu, 2004: Factors responsible for the vertical development of tropical oceanic cumulus convection. *Geophys. Res. Lett.*, **31**, L11109, doi:10.1029/2004GL020225.

Tiedtke, M., 1989: A comprehensive mass flux scheme for cumulus parameterization in large-scale models. *Mon. Wea. Rev*., **117**, 1779–1800.

Tompkins, A. M., 2001: Organization of tropical convection in low vertical wind shears: The role of cold pools. *J. Atmos. Sci.*, **58**, 1650–1672.

Waite, M. L., and B. Khouider, 2010: The deepening of tropical convection by congestus preconditioning. *J. Atmos. Sci.*, **67**, 2601–2615.

Yoneyama, K., 2003: Moisture variability over the tropical western Pacific Ocean. *J. Meteor. Soc. Japan*, **81**, 317–337.

Yoneyama, K., Y. Masumoto, Y. Kuroda, M. Katsumata, K. Mizuno, Y. N. Takayabu, M. Yoshizaki, A. Shareef, Y. Fujiyoshi, M. J. McPhaden, V. S. N. Murty, R. Shirooka, K. Yasunaga, H. Yamada, N. Sato, T. Ushiyama, Q. Moteki, A. Seiki, M. Fujita, K. Ando, H. Hase, I. Ueki, T. Horii, C. Yokoyama, and T. Miyakawa, 2008: MISMO field experiment in the equatorial Indian Ocean. *Bull. Amer. Meteor. Soc.*, **89**, 1889–1903.

Yoneyama, K., C. Zhang, and C. N. Long, 2013: Tracking pulses of the Madden-Julian oscillation. *Bull. Amer. Meteor. Soc.*, **94**, 1871–1891.

Zhang, C., 2005: Madden-Julian Oscillation. *Rev. Geophys*., **43**, RG2003, doi:10.1029/2004RG000158.

Zhang, C., J. Gottschalck, E. D. Maloney, M. W. Moncrieff, F. Vitart, D. E. Waliser, B. Wang, and M. C. Wheeler, 2013: Cracking the MJO nut. *Geophy. Res. Lett.*, **40**, 1223–1230.

Zhang, C., Y. Wang, and K. Hamilton, 2011: Improved representation of boundary layer clouds over the southeast Pacific in ARW-WRF using a modified Tiedtke cumulus parameterization scheme. *Mon. Wea. Rev.*, **139**, 3489–3513.

Zipser, R. J., and M. A. LeMone, 1980: Cumulonimbus vertical velocity events in GATE. Part II: Synthesis and model core structure. *J. Atmos. Sci.*, **37**, 2458–2469.

Zuidema, P., 1998: The 600–800-mb minimum in tropical cloudiness observed during TOGA COARE. *J. Atmos. Sci.*, **55**, 2220–2228.

Zuidema, P., Z. Li, R. J. Hill, L. Bariteau, B. Rilling, C. Fairall, W. A. Brewer, B. Albrecht, and J. Hare, 2011: On trade wind cumulus cold pools. *J. Atmos. Sci.*, **69**, 258–280.